3D Behavior of Schottky Barriers of 2D Transition-Metal Dichalcogenides

Yuzheng Guo[1], *Dameng Liu*[2], *John Robertson*[1]

[1]Department of Engineering, Cambridge University, Cambridge CB2 1PZ, United Kingdom

[2]State Key Laboratory of Tribology, Tsinghua University, Beijing 100084, China

The transition metal dichalcogenides (TMDs) are two-dimensional layered solids with van der Waals bonding between layers. We calculate their Schottky barrier heights (SBHs) using super-cell models and density functional theory. It is found that the SBHs without defects are quite strongly pinned, with a pinning factor S of about S=0.3, a similar value for both top and edge contact geometries. This arises because there is direct bonding between the contact metal atoms and the TMD chalcogen atoms, for both top and edge contact geometries, despite the weak interlayer bonding in the isolated materials. The Schottky barriers largely follow the metal induced gap state (MIGS) model, like those of three-dimensional semiconductors, despite the bonding in the TMDs being largely constrained within the layers. The pinning energies are found to be lower in the gap for edge contact geometries than for top contact geometries, which might be used to obtain p-type contacts on MoS_2.

The transition metal dichalcogenides (TMDs) (MX_2, where M=Mo/W; X=S/Se/Te) are valuable two-dimensional systems, which unlike graphene are semiconductors with a band gap[1] and so are useful for field effect transistors (FETs) [2-16]. They are particularly useful because they make ultra-thin body devices[4] and are suitable for end of the roadmap logic devices such as tunnel FETs (TFETs) [5,6]. The carrier mobilities of TMDs are reasonably high, but it is known experimentally that their device performances tend to be limited by their contact resistance[11, 12]. It appears that most contacts possess Schottky barriers and are not ohmic[11].

There is a desire to control the Schottky barrier heights (SBHs) by varying the contact metal so as to try to minimize contact resistance. Due to the van der Waals inter-layer bonding, it might be expected that the contact metal is also weakly bonded to the MX_2 layer, so that the SBH would vary strongly with contact metal work function, and the Schottky barrier might approach the Schottky limit of weak pinning[17]. This would allow the contact properties to be easily controlled just by varying the metal work function. In practice, this seems not to occur; the SBH seems to be quite strongly pinned[11]. The SBH also seems to depend quite strongly on process conditions, indicating the presence of process-induced defects[18]. Furthermore, the contact Fermi energy is generally pinned in the upper half of the band gap in MoS_2, which favors n-type devices[11]. As bipolar devices are desirable for some applications, it is useful to know if these are possible for MoS_2 itself using high work function electrodes[19, 20], or if different TMDs are needed for p-type devices[14-16].

A better understanding of the Schottky barriers in TMDs is desirable. Fermi level pinning arises from the presence of interface gap states in the TMD which can generally be either due to intrinsic states or to defect states. The least pinning occurs in the defect-free case. There have

been previous calculations of ideal, defect-free SBs for TMDs[21-26], but less extensive than those given here. Here, we provide a comprehensive calculation of Schottky barrier heights of four TMDs with twelve metals (Sc, Mg, Al, Ti, Cr, Mo, Ru, Co, Ni, Pd, Pt, MoO_3) covering a wide range of work functions, for both on-top and edge contact geometries. We show that the defect-free SBHs in fact follow the metal induced gap state (MIGS) model[27-31] that applies to three-dimensional semiconductors, so that relatively strong Fermi level pinning is expected even for defect-free interfaces. Any defects that do form will then cause additional pinning and lower the S value. This insight provides a framework to understand TMD contacts as a whole.

Method

Here, the electronic structure of metal contacts on TMDs is studied directly using density functional theory (DFT) calculations on supercells containing layers of metal and a monolayer of TMD or metal on a block of TMD layers representing the bulk TMD. We use supercells with TMD, metal and no vacuum. We use 6 layers of TMD to represent the bulk TMD, as this is large enough for its gap to be within 0.05 eV of the bulk value[32]. We choose six layers of metal in the face-centered cubic or the body-centered cubic structure. For most metals, the (111) face of the metal is placed on a hexagonal 2x2 supercell of the TMD, and the metal supercell lattice constant is forced to match the TMD cell lattice constant (Fig 1a-c). The metal is allowed to relax perpendicular to the layers, to conserve its volume, which is important because the atomic volume is the main factor determining a metal's work function[33]. For most metals, the lattice mismatch is under 6%, but test calculations with other mismatches in supercells with up to 8x8 lateral cells (0.5% lattice mismatch) were carried out to test the stability of our results. Generally, no symmetry is applied within the supercell, as this allows the contact metal atoms to relax

around the MX_2 atoms. For the Sc case, the Sc atom is much larger and a 1x1 Sc lattice fits on a 2x2 MX_2 supercell. However, here we fix the symmetry for the case of Sc, to stop a reaction between Sc and the MoS_2 which leads to Sc sulfide formation, and which we want to avoid. We also include MoO_3:MoS_2 interfaces to study a high work function case. Here, we use models with a 4×5 supercell of MoS_2 for a good lattice match.

The electronic structure is calculated using the CASTEP plane wave DFT code[34] with the electronic interaction modeled by the PBE style generalized gradient approximation, ultrasoft pseudopotentials and without spin-orbit coupling (not yet included in CASTEP). A cutoff energy of 480 eV converges the total energy to less than 0.01 eV per atom. The DFT errors for van der Waals bonding are corrected using the Grimme[35, 36] scheme. The screened exchange (SX) hybrid functional[37] is used to correct the band gap error of DFT where necessary. Hybrid functionals correct well the band gap error for 3D and bulk 2D semiconductors. But they under-estimate the quasi-particle gap of monolayer 2D semiconductors because of the large exciton energies[38,39] in these poorly screened systems.

The (p-type) Schottky barrier height is the energy difference between the valence band maximum (VBM) and the metal Fermi level, E_f. In practice, this can be difficult to extract from the interface band structures or local density of states because of a strong hybridization between the metal states and the TMD states[22]. We therefore use a reference energy method, in which the Mo 4s or W 5s semi-core level is used as a reference level in the supercell system to derive the metal E_f and the VBM energies from this reference level, and thus the SBH is derived as the difference between these two values. This is the theoretical analogue of Kraut's[40] method in photoemission.

Results and Discussion

Fig. 2 plots the calculated values of the SBHs for monolayer (ML) and bulk MoS_2 against the metal work functions. We used 11 metals to cover a wide range of work functions from Sc (3.5 eV) to Pt (5.65 eV), and we also included MoO_3 at 6.6 eV. The experimental work function values are taken from Michaelson[41]. The SBHs are seen to follow a linear dependence quite closely, despite the different metal reactivities,

$$\phi_p = E_0 + S(\Phi_M - E_0) \qquad (1)$$

Here, E_0 is a reference energy of the gap states that pin the Fermi energies at the SBH. If the pinning is due to intrinsic states such as MIGS, then E_0 would be the charge neutrality level (CNL). The CNL is the energy up to which the MIGS are filled on a neutral surface. The slope $S=d\phi_p/d\Phi_M$ is the pinning factor. It varies between S=1 for unpinned interfaces (Schottky limit) to S=0 for strongly pinned interfaces (Bardeen limit)[28,29]. S can be related for the general case to the density of interface gap states that cause the pinning, N, by[42]

$$S = \frac{1}{1 + \frac{N\delta e^2}{\varepsilon\varepsilon_0}} \qquad (2)$$

where δ is the decay length of these states and $\varepsilon\varepsilon_0$ is the dielectric constant around the interface. Thus, S varies inversely with N, and a large N gives a small S.

In order to display the SBH results for different TMDs, or the bulk and monolayer cases on the same diagrams, we align the bands by their CNLs[27,28] and express the barrier heights with respect to the isotropically averaged CNLs. The CNLs are calculated from the band energies of the isolated semiconductors[30], using the SX band energies to avoid the band gap error (Table 1).

In Fig. 2, we see that the slope S has a similar value for both the monolayer (S=0.28) and bulk (S=0.33) cases. The value of S=0.28 for a monolayer compares to previous calculated values of S~0.3 by Kang et al[25], and by Gong et al[22]. This value of S~0.3 indicates moderate Fermi level pinning. It compares to an experimental value of S=0.1 found by Das et al[11], indicating strong pinning. From Eqn. (2), this stronger pinning than the MIGS model must arise from the presence of extra gap states, and we argue elsewhere[43,44] that these states are due to defects as proposed experimentally[18].

We next consider the edge contact geometry. Here, the metal layer bonds directly to the MX_2 planes. In this geometry, the metals bond directly to the TMD layers via covalent bonds. This geometry is the same as for contacts on three-dimensional semiconductors, so that strong pinning can be expected. The benefits of edge contacts were recently noted for graphene[45], where they greatly increase the effective mobilities. We consider only the monolayer case. There are three possible edge contact geometries for MX_2 as shown in Fig 1(d-f); the non-polar armchair interface where the metal bonds to both Mo and S sites, the zigzag S-terminated interface where the metal bonds to S sites, and the zigzag Mo-terminated interface where the metal bonds to Mo sites.

Fig 3(a) shows the calculated p-type SBHs for these three cases for monolayer MoS_2, referenced to the VBM, and including the SBH values for the top-contact geometry for reference. A notable result is that the slopes S are very similar for all three edge contact cases, and also very similar to that for the top contact case. The similar S values emphasize that the same degree of pinning occurs in each case, which from (2) implies a similar density of gap states is causing the pinning in each case. It suggests that the bonding is quite similar in both cases, as discussed below.

The second notable result is that the SBH value is similar for the three different edge contact geometries, despite the very different bonding types, with unlike or like atom bonds. The typical cause of a shift in barrier heights is the presence of an interfacial dipole layer for the polar interfaces[46]. The absence of a significant shift suggests that the Mo-S bonding is not very polar, and that any dipole is small. Indeed, we calculate a Mulliken charge for MoS_2 of +0.30 e for Mo and –0.15 e for S, indicating that MoS_2 is not very ionic.

A third result is that the p-type SBH is ~0.7 eV lower for edge contacts than for top contacts. As the previous result showed that any dipole layers due to polar bonding are small, we argue that barrier height shift between top and edge contacts is due to the anisotropy of the bonding and crystal field effects. The CNL is the branch point energy of the complex band structure of the semiconductor, where the integral G(E) over the density of band states N(E') is zero[30],

$$G_i(E) = \int_{-\infty}^{\infty} \frac{N(E')dE'}{E-E'} = 0 \qquad (3)$$

This integral is formally taken from -∞ to +∞, as in Tersoff[27]. In practice, it is taken over the energy range of the sulfur 2p states and Mo 4d states, which are the upper 7 valence bands and lower 4 conduction bands[30]. The density N can be further decomposed into angular orbitals, which can take the bonding directional dependence into account.

The integral (3) is single valued for the case of isotropic semiconductors, such as the cubic semiconductors[27,30]. On the other hand, the intra-layer bonding in TMDs is quite anisotropic, so that the partial density of states differs quite considerably for the states of a_1 symmetry bonding along the z direction (relevant to top contacts) to those of e symmetry bonding along the x, y direction[47] (relevant to edge contacts). This is seen in Fig 3(b). We see that the upper valence

band of MoS_2, which is uniquely filled for the trigonal biprism geometry, contains no Mo d_{xz} and d_{yz} states. The Mo states of d_{z2}, d_{x2-y2} and d_{xy} symmetry form peaks directly on either side of the band gap, and so their average energy lies near midgap. On the other hand, the Mo states of d_{xz} and d_{yz} symmetry form density of states peaks away from the gap on the valence band side, so their average is displaced to lower energies, as also seen in ref 47. Thus, the CNL of a_1 states, relevant to top contacts, lies at about 0.7 eV higher energy than the CNL of the *e* symmetry states, relevant to edge contacts (Fig 3b). This accounts for the higher average barrier heights for top contacts. In practical terms, it suggests that more p-type contacts can be implemented for MoS_2 by using the edge contact geomtry.

We now extend the SBH calculations for top-contacts to other TMDs such as monolayer $MoSe_2$, $MoTe_2$ and WS_2 to consider the chemical trends. The same range of metals is used. Fig 4 shows the calculated barrier heights. We see that the calculated pinning factors lie in a similar range. We find that the SBHs on WS_2 have a similar trend of SBH values as in MoS_2, except that the SBHs of $MoSe_2$, $MoTe_2$ and WS_2 are shifted lower in the gap.

We can derive a fitted value of the CNL for top contact on monolayer MoS_2 from Fig 3a as 1.45 eV above the valence band. This assumes an ionization potential (IP) of 5.98 eV for ML MoS_2, derived from the experimental IP of bulk MoS_2 of 5.47 from Jaegermann et al[48], allowing for the VB shift with layer number. The fitted CNL value is within 0.05 eV of the calculated value in right margin of Fig 3a.

Monch[28] noted that the pinning factors of different 3D semiconductors obeyed an empirical relationship

$$S = \frac{1}{1 + 0.1(\varepsilon_\infty - 1)^2} \qquad (4)$$

where ε_∞ is the optical dielectric constant. The pinning factor for $MoTe_2$ is lower than in MoS_2 because of its narrower band gap and larger ε_∞ value, according to (4).

Fig. 5 shows that the experimental SBH values of 3D semiconductors follow this dependence (4) quite well. Taking the optical dielectric constants of TMDs from the literature[49], we can plot the S versus ε_∞ in Fig. 5 according to eq (4). The data points follow relationship (4) reasonably closely but lie slightly below the 3D line. The slope is quite similar. It is interesting to see that old experimental data points for the 2D GaS-GaTe series of Kurtin[50] have a similar slope to the 3D semiconductors.

The combination of experimental data for 3D semiconductors, our calculated S values for TMDs, and previous data for the GaS 2D semiconductors suggest that all three families follow a similar model, the MIGS model. However, for a given ε_∞, the (1/S) - 1 value is shifted lower for the 2D GaS family and the 2D TMDs, corresponding to a lower net density of MIGS (N) in equation (2).

We now explain why the TMDs tend to follow the MIGS model, despite their two-dimensional bonding. It is because the top contact metal atoms strongly bond to the TMDs, and the contact metal to chalcogen bonds are as short as in the edge contacts. The bond lengths between contact metals and the S sites of MoS_2 are shown in Fig 6(a). The intra-layer Mo-S bond length is 2.41Å. The bond lengths for top contacts cover a range, due to the lower symmetry. For the shortest distance, the bond length is the same as for the edge contacts, Fig 6(a). Thus, there is mostly strong bonding between the contact metal atoms and the S atoms. It is not van der Waals bonding. Interestingly, the presence of top contact bonds does not disrupt the intra-layer M-X bonds of the MoS_2 or WS_2 layer, because MoS_2 and WS_2 are both strongly bonded systems with a large heat of formation[44], Mo and W being at the center of the transition metal series. The

second point is that the chalcogens are third or higher row elements and their atoms can over-coordinate without affecting the interlayer bonding of MoS_2. They are not like C atoms in graphene. Thus, the pinning factors, the similarity of top and edge contacts, and the contact atom bond lengths all support the idea that MX_2 SBHs follow the standard MIGS model. The MIGS states themselves can be seen as gap states decaying away from the electrode interface in Fig 6(b).

Experimentally, the preparation of contacts can lead to the creation of defects. These give rise to extra pinning as seen by the experiments of Das[11] and McDonnell[18]. The effect of defects on SBHs in these systems has been studied theoretically by Liu et al[43] and Guo et al[51]. The different SBH between top and edge contacts could also introduce a local variation of SBHs and might also account for the data of McDonnell[18].

Finally, we considered MoO_3/MoS_2 contacts for the extremely high work function case. O-deficient MoO_3 is a degenerate n-type semiconductor with a work function of 6.6 eV[50]. Fig 7(a,b) shows the O-rich and non-polar MoO_3 faces. The non-polar face gives a SBH that falls on the trend line in Fig 2. The O-rich interface gives a much more p-type SBH, closer to the valence band, Fig 7c. Thus, MoO_3 electrode is a valuable method to give a hole contact, as found by experiment[19]. The introduction of O vacancies, moving from the O rich interface towards the non-polar interface leads to a large change in SBH.

In summary, the contact problem for 2D TMDs has been studied by detailed DFT calculations. A strong Fermi level pinning effect is found for all defect-free metal:TMD interfaces. The calculated Schottky barrier heights follow the standard MIGS model, despite van der Waals inter-layer bonding. The strong pinning occurs because the contact metal atoms are quite strongly bonded to the S atoms of MoS_2, even for top contacts, while not disturbing the intra-

layer Mo-S bonding. The Fermi level is pinned near the conduction band for MoS_2 and nearer midgap for other 2D TMDs. The pinning factor is 0.3 for MoS_2 and is lower for other 2D materials. This explains why most MoS_2 MOSFETs are n-type. Defects increase the pinning, and reduce the dependence of SBH on contact metal work function even further, and shift the pinning energy towards the anion vacancy defect level.

The authors acknowledge the financial support of EPSRC grant EP/J011592.

References

1. Mak, K. F.; Lee C.; Hone, J.; Shan, J.; and Heinz, T. F. Atomically Thin MoS_2: A New Direct-Gap Semiconductor. *Phys. Rev. Lett.* 2010, 105, 136805.

2. Radisavljevic, B.; Radenovic, A.; Brivio, J.; Giacometti, V.; Kis, A. Single-layer MoS_2 transistors. *Nat. Nanotechnol.* 2011, 6, 147-150.

3. Butler, S. Z.; Hollen, S. M.; Cao, L.; Cui, Y.; Gupta, J. A.; Gutiérrez, H. R.; Heinz, T. F.; Hong, S. S.; Huang, J.; Ismach, A. F.; et al. Progress, Challenges, and Opportunities in Two-Dimensional Materials Beyond Graphene. *ACS Nano* 2013, 7, 2898–2926.

4. Yoon, Y.; Ganapathi, K.; Salahuddin, S. How Good Can Monolayer MoS_2 Transistors Be? *Nano Lett.* 2011, 11, 3768–3773.

5. Das, S.; Prakash, A.; Salazar, R.; Appenzeller, J. Toward Low-Power Electronics: Tunneling Phenomena in Transition Metal Dichalcogenides. *ACS Nano* 2014, 8 1681-1689.

6. Fiori, G.; Bonaccorso, F.; Iannaccone, G.; Palacios, T.; Neumaier, T.; Seabaugh, A.; Banerjee, S.K.; Colombo, L.; Electronics based on two-dimensional materials. *Nat. Nanotechnol.* 9 768 (2014)

7. Kim, S.; Konar, A.; Hwang, W.; Lee, J.; Lee, J.; Yang, J.; Jung, C.; Kim, H.; Yoo, J.; Choi, J.; Jin, Y.; *et al*. High-mobility and low-power thin-film transistors based on multilayer MoS_2 crystals. *Nat. Commun.* 2012, 3, 1011.

8. Wu, W.; De, D.; Chang, S.C.; Wang, Y.N.; Peng, H.B.; Bao, J.M.; Pei, S.S. High mobility and high on/off ratio field-effect transistors based on chemical vapor deposited single-crystal MoS_2 grains. *Appl. Phys. Lett.* 102 142106 (2013).

9. Zhang, Y. J.; Ye, J. T.; Matsuhashi, Y. and Iwasa Y. Ambipolar MoS_2 Thin Flake Transistors. *Nano. Lett.* 2012, 12, 1136-1140.

10. Liu, H.; Neal, A. T.; Ye, P. D.; Channel Length Scaling of MoS_2 MOSFETs. *ACS Nano* 2012, 6 8563-8569.

11. Das, S.; Chen, H. Y.; Penumatcha, A. V. and Appenzeller J., High Performance Multilayer MoS_2 Transistors with Scandium Contacts. *Nano. Lett.* 2013, 13, 100-105.

12. Pradhan, N. R.; Rhodes, D.; Zhang, Q.; Talapatra, S.; Terrones, M.; Ajayan, P. M.; Balicase, L. Intrinsic carrier mobility of multi-layered MoS2 field-effect transistors on SiO_2. *Appl. Phys. Lett.* 2013, 102, 123105.

13. Bao, W.;Cai, X.; Kim, D.; Sidhara, K.; Fuhrer, M. S. High mobility ambipolar MoS_2 field-effect transistors: Substrate and dielectric effects. *Appl. Phys. Lett.* 2013, 102, 042104.

14. Das, S.; Appenzeller, J. WSe_2 field effect transistors with enhanced ambipolar characteristics. *Appl. Phys. Lett.* 2013, 103, 103501.

15. Liu, W.; Kang, J. H.; Sarkar, D.; Khatami, Y.; Jena, D. and Banerjee, K. Role of Metal Contacts in Designing High-Performance Monolayer n-Type WSe_2 Field Effect Transistors. *Nano. Lett.* 2013, 13, 1983-1990.

16. Zhang, W.; Chiu, M.; Chen, C.-H.; Chen, W.; Li, L.-J.; Wee, A. T. S. Role of Metal Contacts in High-Performance Phototransistors Based on WSe_2 Monolayers. *ACS Nano*, 2014, 8, 8653.

17. Lince, J. R.; Carre, D. J.; Fleischauer, P. D. Schottky-Barrier Formation on a Covalent Semiconductor without Fermi-Level Pinning: The Metal-MoS_2(0001) Interface. *Phys. Rev. B* 1987, 36, 1647.

18. McDonnell, S.; Addou, R.; Buie , C.; Wallace, R. M.; Hinkle, C L. Defect-Dominated Doping and Contact Resistance in MoS_2. *ACS Nano*, 2014, 8, 2880–2888.

19. Chuang, S.; Battaglia, C.; Azcatl, A.; McDonnell, S.; Kang, J. S.; Yin, X.; Tosun, M.; Kapadia, R.; Fang, H.; Wallace, R. M.; Javey, A.; MoS_2 P-type Transistors and Diodes Enabled by High Work Function MoO_x Contacts. *Nano Lett.* 2014, 14, 1337-1342.

20. McDonnell, S.; Azcatl, A.; Addou, R.; Gong, C.; Battaglia, C.; Chuang, S.; Cho, K.J.; Javey, A.; Wallace, R.M.; ACS Nano 8 6265 (2014)

21. Popov, I.; Seifert, G.; Tomanek, D. Designing Electrical Contacts to MoS_2 Monolayers: A Computational Study. *Phys. Rev. Lett.* 2012, 108, 156802.

22. Gong, C.; Colombo, L.; Wallace, R M.; Cho, K. J. The Unusual Mechanism of Partial Fermi Level Pinning at Metal–MoS_2 Interfaces. *Nano Lett.*, 2014, 14, 1714-1720.

23. Chen, W.; Santos, E. J. G.; Zhu, W. G.; Kaxiras, E.; Zhang, Z. Y. Tuning the Electronic and Chemical Properties of Monolayer MoS_2 Adsorbed on Transition Metal Substrates. *Nano Lett*. 2013, 13, 509-514.

24. Cakir, D.; Peeters, F. M.; Dependence of the electronic and transport properties of metal-$MoSe_2$ interfaces on contact structures. *Phys. Rev. B* 2014, 89, 245403.

25. Kang, J.; Liu, W.; Sarkar, D.; Jena, D.; Banerjee, K.; Computational Study of Metal Contacts to Monolayer Transition-Metal Dichalcogenide Semiconductors. *Phys. Rev. X* 2014, 4, 031005.

26. Y Guo, J Robertson, Schottky barrier heights and band alignments in transition metal dichalcogenides. *Microelec. Eng.* 2015, 147, 184-187.

27. Tersoff, J. Schottky Barrier Heights and the Continuum of Gap States. *Phys. Rev. Lett.* 1984, 52, 465.

28. Mönch, W. Role of Virtual Gap States and Defects in Metal-Semiconductor Contacts. *Phys. Rev. Lett.* 1987, 58, 1260.

29. Mönch, W. Metal-Semiconductor Contacts: Electronic Properties. *Surf. Sci.* 1994, 300, 928-944.

30. Robertson, J. Band Offsets of Wide-Band-Gap Oxides and Implications for Future Electronic Eevices. *J. Vac. Sci. Technol. B* 2000, 18, 1785-1791.

31. Robertson, J. Band offsets, Schottky barrier heights, and their effects on electronic devices. *J. Vac. Sci. Technol. A* 2013, 31, 050821.

32. Ellis, J. K.; Lucero, M J.; Scuseria, G. E.; The Indirect to Direct Band Gap Transition in Multilayered MoS_2 as Predicted by Screened Hybrid Density Functional Theory. *Appl. Phys. Lett.* 2011, 99, 261908.

33. Lang, N.D.; Kohn, W. Theory of Metal Surfaces: Work Function. *Phys. Rev. B* 1971,3, 1215.

34. Clark, S. J.; Segall, M. D.; Pickard, C. J.; Hasnip, P. J.; Probert, M. J.; Refson, K., Payne, M. C. First principles methods using CASTEP. Zeitschrift für Kristallographie - Crystalline Materials. 2005, 220, 567-570.

35. Grimme, S. Semiempirical GGA-type density functional constructed with a long-range dispersion correction. *J. Comp. Chem.* 2006, 27, 1787-1799.

36. McNellis, E. R.; Meyer, J.; Reuter, K. Azobenzene at coinage metal surfaces: Role of dispersive van der Waals interactions. *Phys. Rev. B* 2009, 80 205414.

37. Clark, S.J.; Robertson, J Screened Exchange Density Functional Applied to Solids. *Phys. Rev. B* 2010, 82, 085208.

38. Cheiwchanchamnangij, T.;Lambrecht, W. R. L. Quasiparticle band structure calculation of monolayer, bilayer, and bulk MoS_2. *Phys. Rev. B* 2012, 85, 205302.

39. Ramasubramaniam, A. Large Excitonic Effects in Monolayers of Molybdenum and Tungsten Dichalcogenides. *Phys. Rev. B* 2012, 86, 115409.

40. Kraut, E. A.; Grant, R. W.; Waldrop, J. R.; Kowalczyk, S. P. Precise Determination of the Valence-Band Edge in X-Ray Photoemission Spectra: Application to Measurement of Semiconductor Interface Potentials. *Phys. Rev. Lett.* 1980, 44,1620.

41. Michaelson, H.B. The Work Function of the Elements and Its Periodicity. *J. Appl. Phys.* 1977, 48, 4729.

42. Cowley, A. W.; Sze, S. M.; Surface States and Barrier Height of Metal‐Semiconductor Systems. *J. Appl. Phys.* 1965, 36, 3212.

43. Liu, D.; Guo, Y.; Fang, L.; Robertson, J. Sulfur Vacancies in Monolayer MoS_2 and Its Electrical Contacts. *Appl. Phys. Lett.* 2013, 103, 183113.

44. Guo, Y.; Liu, D.; Robertson, J. Chalcogen vacancies in monolayer transition metal dichalcogenides and Fermi level pinning at contacts. *Appl. Phys. Lett.* 2015, 106, 173106.

45. C. Gong, S. McDonnell, X. Qin, A. Azcati, H. Dong, Y.J. Chabal, K.J. Cho, R. M. Wallace, ACS Nano 8, 642 (2014).

46. Tse, K.Y.; Robertson, J. Control of Schottky Barrier Heights on High-K Gate Dielectrics for Future Complementary Metal-Oxide Semiconductor Devices. *Phys. Rev. Lett.* 2006, 99, 086805.

47. Yue, Q.; Shao, Z.; Zhang, X.; Chang, S.; Wang G.; Qin, Q.; Li, J.; Mechnaical and electronic properties of monolayer MoS under elastic strain. *Phys. Lett. A 2012, 376,1166-1170.*

48. Schlaf, R.; Lang, O.; Pettenkofer, C.; and Jaegermann, W.; Band Lineup of Layered Semiconductor Heterostructures prepared by Van der Waals Epitaxy, *J Appl Phys 1999, 85, 2732*.

49. Bell, M. G.; Liang, W. Y. Electron energy loss studies in solids; The transition metal dichalcogenides. *Adv. Phys.* 1976, 25, 53-86;

50. Kurtin, S.; Mead, C. A. Surface Barriers on Layer Semiconductors: GaS, GaSe, GaTe. *J. Phys. Chem. Solids* 1969, 30, 2007.

51. Guo, Y.; Robertson, J. Origin of the high work function and high conductivity of MoO_3 *Appl. Phys. Lett.* 2014, 105, 222110.

Table 1 Comparison of band gaps calculated by GGA and SX, and the isotropically averaged CNL values calculated from the SX bands.

eV	Band gap		Isotropic CNL
	GGA	SX	calculated
MoS_2-ML	1.55	1.88	0.95
$MoSe_2$-ML	1.53	1.71	0.84
$MoTe_2$-ML	1.38	1.46	0.72
WS_2-ML	1.94	2.13	1.07
WSe_2-ML	1.64	1.82	0.73
WTe_2-ML	1.55	1.31	0.63
MoS_2-3D	0.97	1.3	0.70
$MoSe_2$-3D	0.95	1.16	0.43
$MoTe_2$-3D	0.78	1.01	0.33
WS_2-3D	1.17	1.44	0.88
WSe_2-3D	1.15	1.33	0.77
WTe_2-3D	1.01	1.07	0.39

Figure captions

1 Bonding at (a) Ti-MoS_2, (b) Cr –MoS_2, (c) Ni-MoS_2 top contacts. Mo= cyan, S= yellow, metal blue/grey. Edge metal-MoS_2 contacts, top views. (d) non-polar armchair, (e) S-terminated zigzag, (f) and Mo terminated zigzag. Mo=cyan, S = yellow, metal =purple.

2. Comparison of calculated Schottky barrier heights for top contacts on bulk and monolayer MoS_2 in GGA, referenced to their charge neutrality levels. Monolayer data and band edges = red, bulk data and band edges = black.

3(a) Calculated p-type SBHs for the three edge-contacted ML MoS_2 interface, compared to the case of top-contacted ML MoS_2, referenced to valence band maximum. Note the similar pinning factors S for each case. (b) Calculated Mo d density of states separated into angular components, showing the different contributions to the bands.

4. Comparison of calculated p-type barrier heights for monolayer MoS_2, $MoSe_2$, $MoTe_2$ and WS_2 refered to their CNLs. Colors of data points, fit, and band edges for each compound.

5. Experimental values of pinning factors S for 3D semiconductors, for the 2D series GaS, GaSe and GaTe ref 49), and our calculated values of pinning factors for bulk MoS_2, $MoSe_2$, $MoTe_2$ and WS_2 plotted against optical dielectric constant.

6. (a) Comparison of contact metal – S bond lengths for top and edge contacts for various metals on MoS_2. (b) Partial density of states at MoS_2 layers away from a Ni/MoS_2 interface, showing the decay of the metal induced gap states.

7 (a,b) MoO_3 O-rich and non-polar interfaces with MoS_2. O=red, Mo=cyan, S= yellow. (c) Calculated Schottky barrier heights for O-rich and non-polar MoO_3 faces on monolayer MoS_2

and WS_2, referred to VB edge. For MoS_2 we have also included the O-rich surface with O vacancy defect at the MoO_3 interface, labeled as V_O.

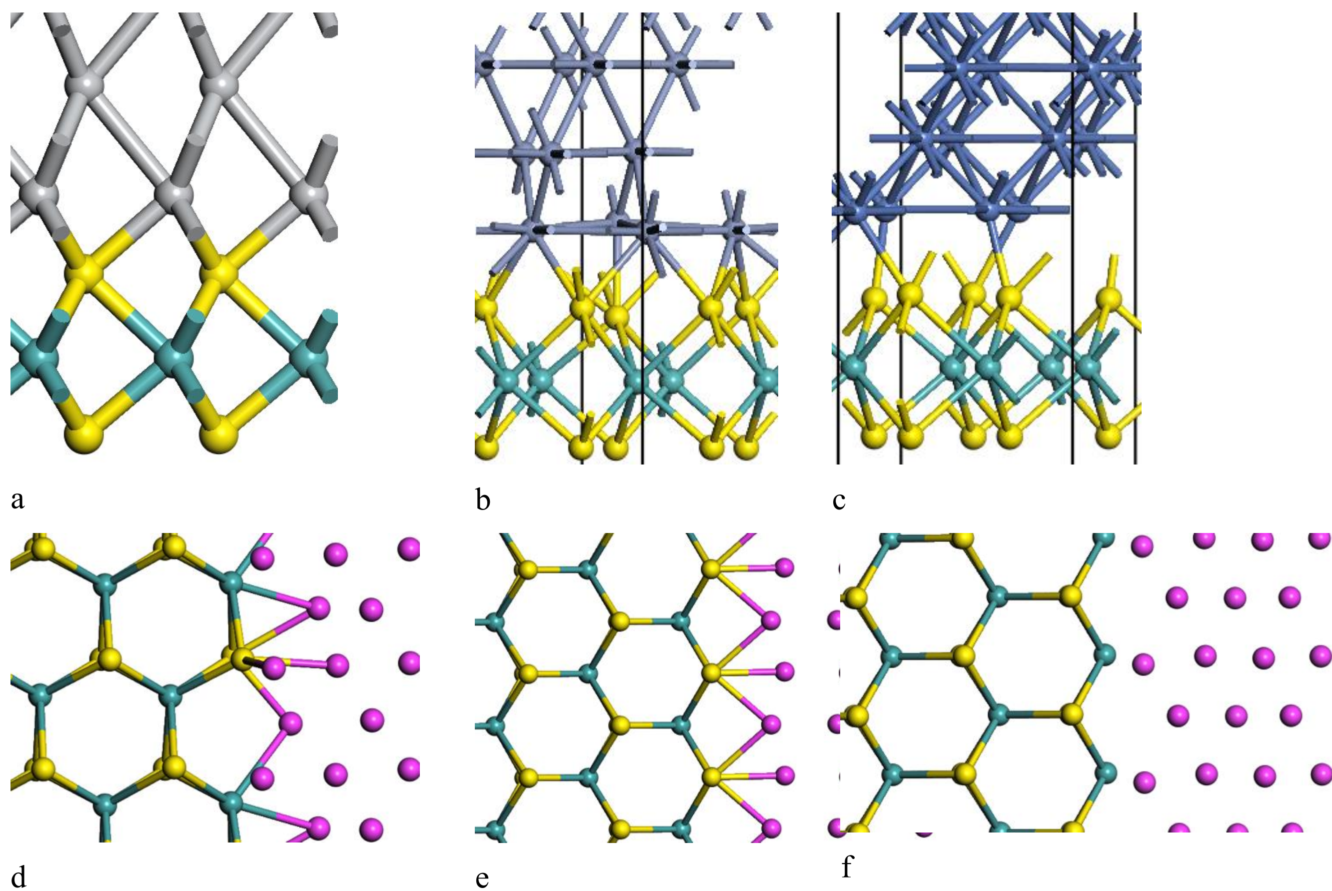

Fig. 1.

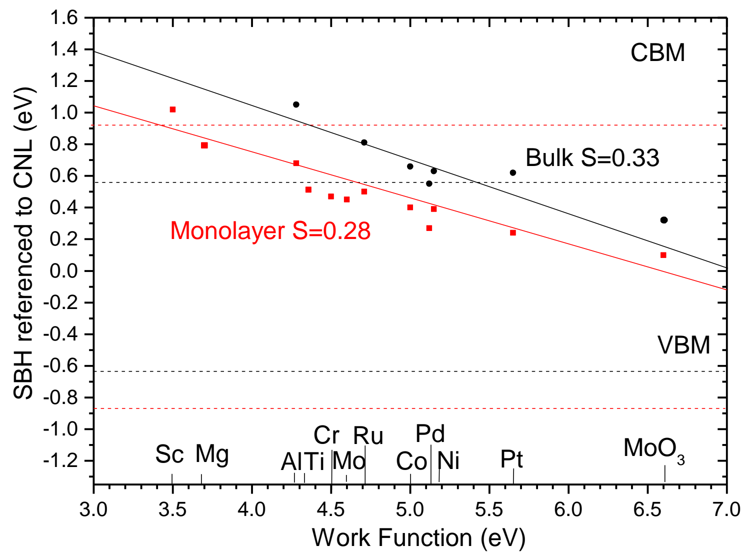

Figure 2

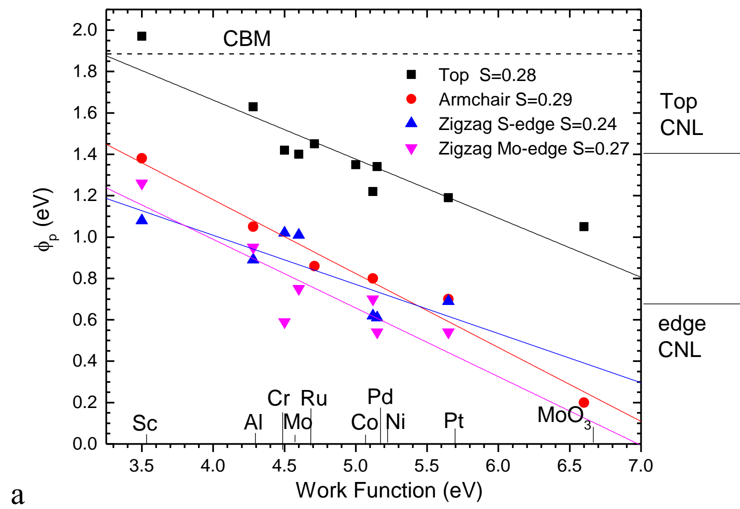

a

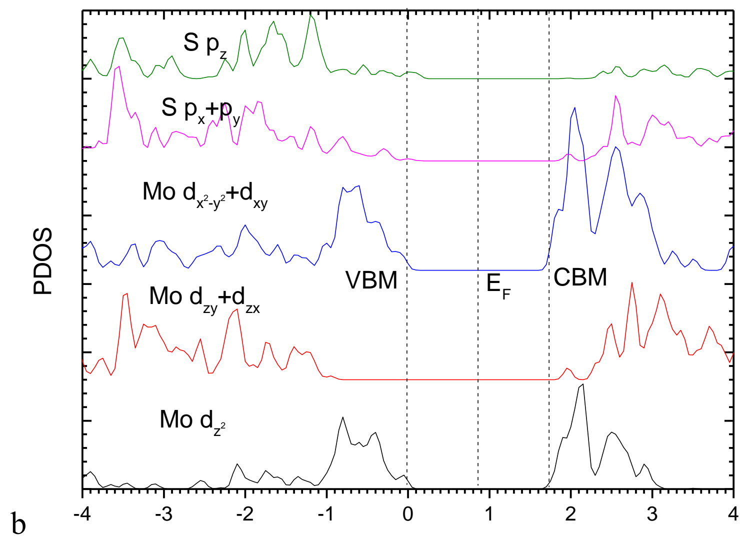

b

Figure 3

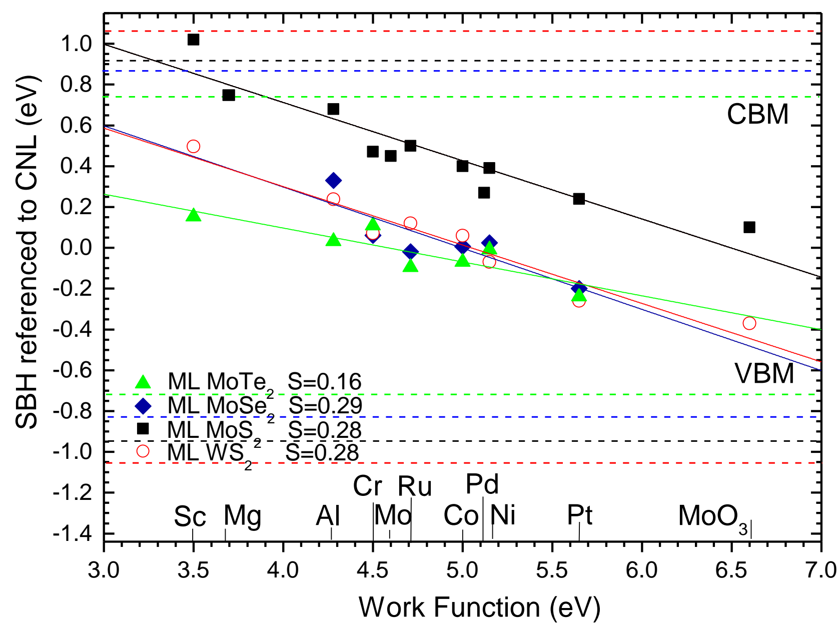

Fig. 4.

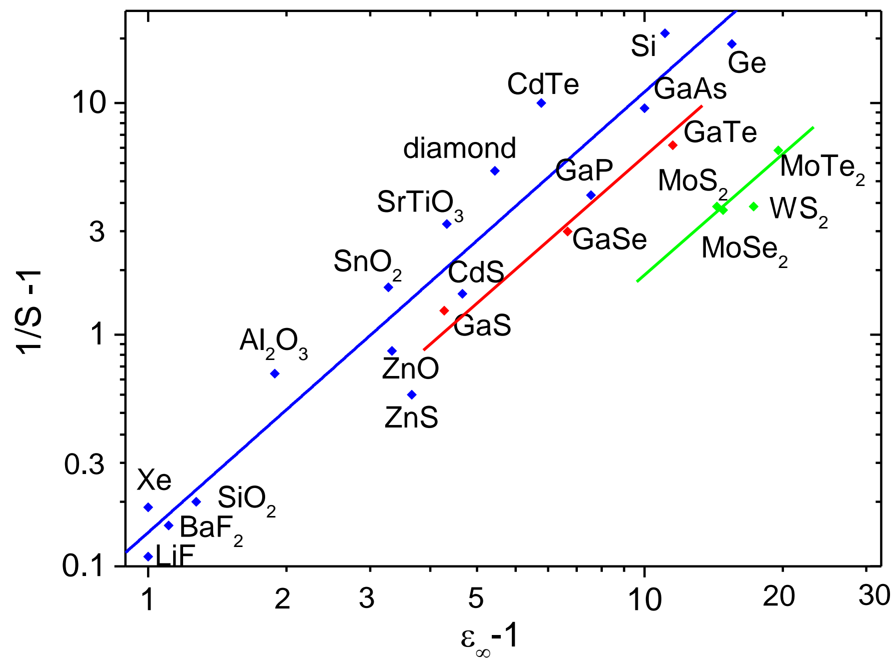

Fig. 5

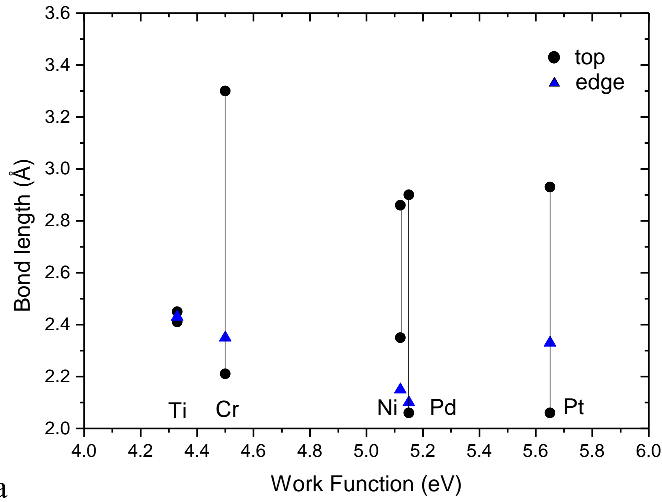

a

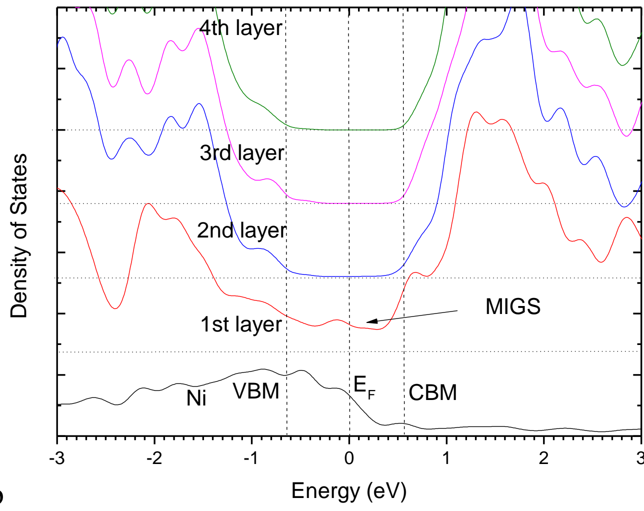

b

Figure 6

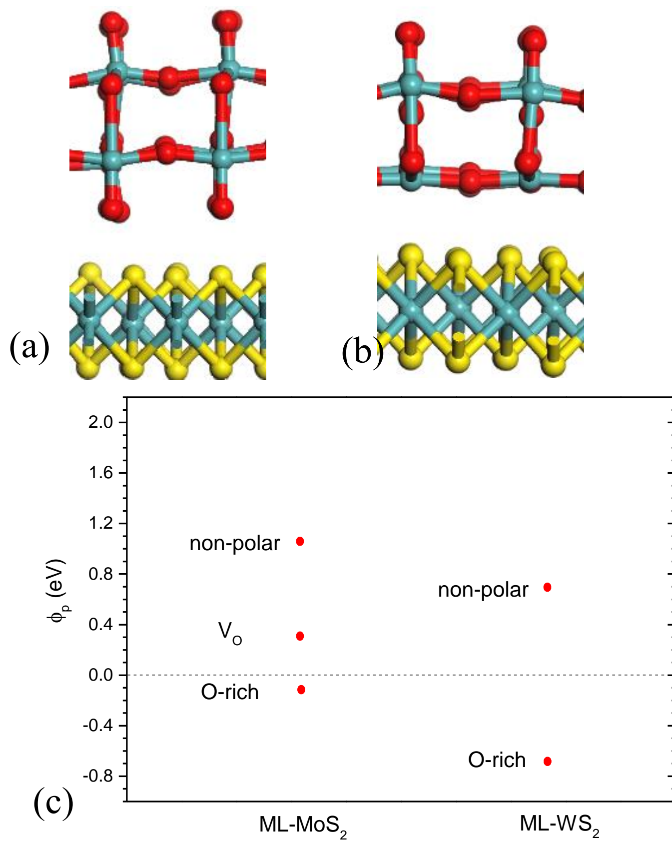

Figure 7